Sensors & Actuators: A. Physical 396 (2025) 117134

Contents lists available at ScienceDirect

Sensors and Actuators: A. Physical

journal homepage: www.journals.elsevier.com/sensors-and-actuators-a-physical

Machine learning-enabled triboelectric nanogenerator for self-powered condition monitoring and regulation of USV-ROV umbilical cable

Yan Yang [a], Xingjia Jiang [a,*], Hengxu Du [a], Fangyang Dong [a], Mengwei Wu [a], Qiang Zhao [a,b], Taili Du [a,*], Minyi Xu [a,*]

[a] *Dalian Key Lab of Marine Micro/Nano Energy and Self-Powered Systems, Marine Engineering College, Dalian Maritime University, Dalian 116026, China*
[b] *College of Mechanical and Control Engineering, Baicheng Normal University, Baicheng, Jilin 137000, China*

ARTICLE INFO

Keywords:
USV-ROV
Umbilical cable
Support Vector Machines
Triboelectric nanogenerators

ABSTRACT

The umbilical cable is a critical component of the Unmanned Surface Vehicle–Remotely Operated Vehicle (USV-ROV) collaborative system, which faces damage caused by stretching during operations. In this work, a triboelectric sensor (U-TENG), composed of flexible silicone rubber and spiral electrodes, for in-situ umbilical cable condition monitoring is proposed for the first time. Then, an integrated self-powered cable condition monitoring and regulation system is constructed to recognize different signal for different working condition based on machine learning-enabled U-TENG. Even more, the actuator controls the winch bidirectionally to regulate cable tension and provide closed-loop responses to abnormal conditions. Experimental results demonstrate that the U-TENG maintains stable electrical output across a strain range of 0–100 % and excitation frequencies of 0.5–4.0 Hz, while also demonstrating high sensitivity to bending deformation. Cable status monitoring accuracy achieves 97.18 % under 16 operating conditions. In addition, the proposed system demonstrates excellent responsiveness in underwater environment, preventing damage to the umbilical cable due to overload effectively. Thus, the proposed triboelectric sensor and control system hold significant potential for realizing ROV umbilical cable condition sensing and enhancing the safety of USV-ROV operational platforms.

1. Introduction

With the rapid advancement of technology, human exploitation and utilization of marine resources have steadily increased, driving more frequent marine engineering activities. Unmanned Surface Vehicle–Remotely Operated Vehicle (USV-ROV) collaborative systems have been widely employed in areas including coastal hydrographic surveying [1,2], underwater infrastructure inspection [3], and military reconnaissance [4]. The umbilical cable, a critical component linking the USV and ROV, fulfills diverse roles such as power transmission, data communication, and dynamic towing [5,6]. However, in practical operations, umbilical cables are susceptible to damage from stretching, bending, or twisting [7,8], potentially causing the ROV to lose control or the USV to be dragged, resulting in severe safety incidents. Therefore, real-time and accurate monitoring of the umbilical cable's condition is essential for risk warning, proactive tension regulation, and ensuring the safe operation of the system.

Current umbilical cable condition detection mainly relies on five methods: Tether Management Systems (TMS) [9,10], machine vision [11], kinematic simulation [12–15], conventional sensors [16], and mechanical structural methods [8,12,17]. For instance, B.A. Abel et al. [10] employed a TMS to adjust the umbilical cable length, effectively alleviating the cable's self-weight resistance and enhancing its adaptability in complex sea conditions; Matheus et al. [11] developed a vision-based servo monitoring system for real-time umbilical cable condition monitoring, which was used to achieve relative positioning among multiple ROVs; Chen et al. [14] developed a dynamic model for umbilical cables under complex sea conditions using Kirchhoff's bar theory. Their work analyzed the cables' dynamic characteristics across different sea states to prevent breakage caused by the combined effects of mothership movement and ocean currents. Ornella Tortorici et al. [16] proposed an active control system for umbilical cables integrating bending sensors, utilizing a two-layer structure combining a passive compliant mechanism with an active feeder to achieve precise dynamic adjustment of cable length; Christophe Viel et al. [18] utilized a sliding buoy to dynamically straighten the cable, combined with a geometric

---

* Corresponding authors.
E-mail addresses: jiangxj@dlmu.edu.cn (X. Jiang), dutaili@dlmu.edu.cn (T. Du), xuminyi@dlmu.edu.cn (M. Xu).

https://doi.org/10.1016/j.sna.2025.117134
Received 3 August 2025; Received in revised form 24 September 2025; Accepted 4 October 2025

model to predict its shape. This method requires no active drive system and relies solely on buoyancy and gravity for adaptive cable adjustment, thereby reducing equipment complexity and operational difficulty. These studies have achieved significant progress in umbilical cable monitoring, but these methods still face formidable challenges such as heavy dependence on power supplies, complex model computations, and limited environmental adaptability, which impede the achievement of real-time cable condition monitoring.

In recent years, triboelectric nanogenerators (TENG) have emerged as a novel self-powered sensing technology characterized by high sensitivity, low cost, and ease of fabrication [19,20], They have been widely employed in fields including robotic perception [21–27], wearable devices [28–31], energy harvesting [32–34], and industrial monitoring [35–37]. Operating on the principles of triboelectric charging and electrostatic induction, TENG directly converts mechanical energy into electrical signals without requiring external power [38–41]or complex data processing, making it a promising solution for dynamic umbilical cable monitoring. More importantly, the flexible design of triboelectric sensors allows customization according to application requirements [42,43], including solid-liquid TENG [44,45], liquid-liquid TENG [46,47], flexible TENG [48], etc. thereby improving their adaptability in complex environments.

Umbilical cables frequently sustain mechanical loads such as stretching and bending during underwater operations, making the development of sensors capable of detecting these deformations crucial for ensuring operational safety. Currently, TENG technology demonstrates significant potential for detecting stretching and bending deformations and is widely used in wearable devices to sense changes caused by human movements. For example, Yi et al. [49] developed a stretchable silicone rubber-based triboelectric sensor to monitor human motion and respiration. This sensor detects surface charge changes induced by material deformation and outputs corresponding electrical signals. However, the variable stretching directions in human movement differ from the predominantly axial loading of umbilical cables. Faced with a more complex marine environment, Zhao et al. [50] proposed an R-TENG composed of highly elastic latex tubes and silicone rubber, which has good flexibility, stretchability, and water resistance, and has been applied to the condition monitoring of marine structures. These efforts have demonstrated that TENG can monitor tension and deformation, so TENG is expected to solve the difficult problem of umbilical cables, which are mainly subject to localized impact tension. This work not only achieves accurate differentiation between tensile and bending modes but also integrates a real-time classification system based on machine learning with a winch control system. This forms a complete “sensing-recognition-execution” closed-loop architecture capable of autonomously adjusting cable tension under wave interference, effectively preventing overload damage. It provides a new approach for umbilical cable condition monitoring in complex marine environments.

Based on the TENG principle, this study presents a triboelectric sensor for umbilical cable condition monitoring (U-TENG) and a corresponding self-regulating system. Unlike energy harvesting efforts [51,52] focused on efficiency optimization, the core distinction lies in addressing the state identification and active control of umbilical cables in dynamic marine environments, rather than merely optimizing energy harvesting efficiency. Unlike most TENG sensors that rely on monitoring output voltage amplitude, this study effectively circumvents the inherent drawback of amplitude susceptibility to environmental interference by analyzing waveform characteristics and integrating machine learning algorithms. This approach provides a novel strategy for achieving stable and reliable umbilical cable status recognition. The U-TENG monitors umbilical cable stretching and bending states, while the self-regulating system analyzes sensor signals and controls winch operation, enabling real-time tension control. The U-TENG consists of flexible silicone rubber, two layers of spiral electrodes, a sealing layer, and a mounting frame. It has excellent elasticity and does not affect the original mechanical properties of the cable body after being embedded in it. Cable deformation causes the internal electrodes of the U-TENG to meet or separate from the dielectric layer, generating triboelectric signals. The microcontroller collects and filters the signal before feeding it into a machine learning model for real-time identification of stretching or bending states. Based on the identification results, the system converts the triboelectric signals into commands that control the winch’s forward and reverse rotation, enabling active regulation of the umbilical cable’s tension to prevent damage or breakage due to excessive force. Experimental results show that the U-TENG outputs stable signals within a 0–100 %(0–10 cm) stretching range, exhibit good linearity, has high sensitivity to bending, and maintains stable performance under various excitation conditions. Through simulation experiments, the feasibility of the umbilical cable condition monitoring and autonomous control system was verified. This work constructed a closed-loop system comprising signal sensing, status recognition, and adaptive control, providing a new solution for the safe operation of ROV umbilical cables in complex sea conditions.

2. Results and discussion

2.1. Structure and working principle of U-TENG

The U-TENG is installed near the umbilical cable’s connection point to the ROV (Fig. 1a) for real-time monitoring of the stress states in critical regions. When sudden tension changes occur due to umbilical cable entanglement or abnormal ROV attitudes, the sensor generates triboelectric signals in response to stretching, enabling real-time warning. Fig. 1b shows a schematic diagram of the sensor installation, which ensures efficient response to external mechanical stimuli without damaging the umbilical cable structure.

The U-TENG exhibits high elasticity under stretching (Fig. 1c) and can tolerate a 0–100 % strain range, satisfying underwater operational requirements. As shown in Fig. 1d(i), the U-TENG responds rapidly to external tensile forces underwater, with excellent response speed during both loading and unloading—forming the basis for state identification. Furthermore, Fig. 1d(ii) illustrates the signal processing workflow: a microcontroller collects triboelectric signals, which are then processed by a machine learning model for state recognition. Once abnormal stretching is detected, the system can automatically control the winch to adjust cable tension, thereby preventing cable breakage. Additionally, to enhance operational convenience, an Organic Light-Emitting Diode (OLED) display is integrated to visualize monitoring results, allowing on-site personnel to respond promptly.

To withstand the combined tensile and bending loads on the umbilical cable, the sensor body is constructed from elastic silicone rubber, ensuring compatibility with its operating environment. The preparation process of the U-TENG body is shown in Fig. 2a: First, components A and B of Ecoflex 00–10 are mixed in a 1:1 wt ratio. Following 5-minute vacuum degassing, the mixture is injected into a mold (length: 100.0 mm; inner diameter: 13.0 mm) and cured at 40°C for 3 h to form the first inner core silicone rubber layer. Next, 20 turns of copper wire with a 2.0 mm diameter are uniformly wound around the surface, forming the first sensing electrode layer. Then, the second layer of Dragon Skin 00–30 silicone rubber is poured into the mold (inner diameter 15.5 mm), serving both as a support layer and a friction layer. After curing, another 20 turns of copper wire of the same specification are wound around to form the second sensing electrode layer. Finally, a third silicone rubber layer is poured using a mold with a 20.0 mm inner diameter to form the outer protective layer. K-704 organic silicone sealant is then evenly applied to the surface to enhance waterproof performance. Additionally, after curing, the organic silicone adhesive forms a dense silicone layer that effectively isolates the internal sensitive components from direct contact with seawater, thereby significantly reducing the impact of salinity on the U-TENG output.

The overall structure of the U-TENG is shown in Fig. 2b. The fixture’s elbow aperture is custom-designed to match the ROV umbilical cable

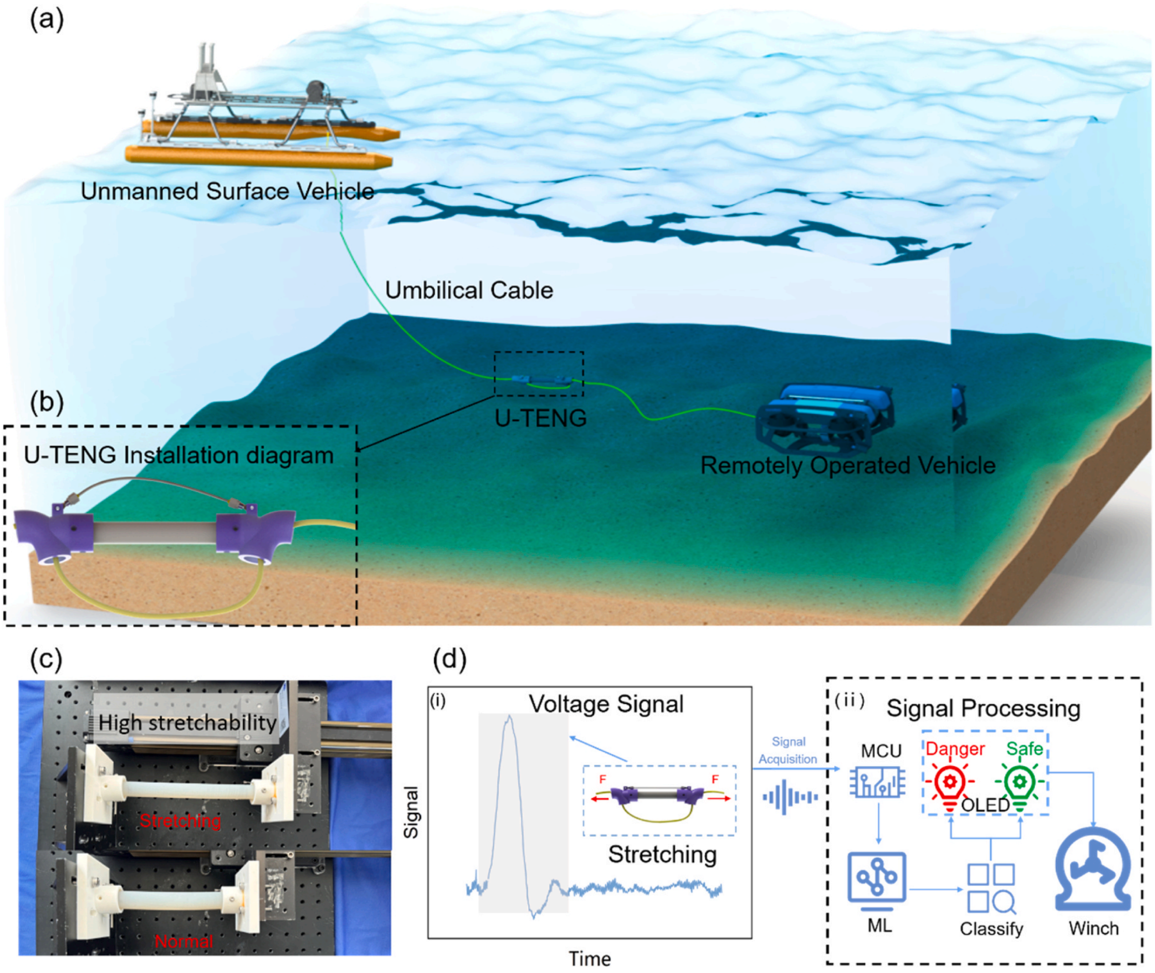

Fig. 1. U-TENG applications, characteristics, and signal processing. (a) U-TENG application scenarios. (b) U-TENG installation diagram. (c) U-TENG characteristics. (d)(i) Device output characteristics; (ii) U-TENG signal processing.

diameter (0.8 cm), ensuring a tight fit around the cable. The U-TENG body is embedded between the two mounting brackets and secured with screws to ensure a firm fit. The mounting brackets are equipped with steel cable mounting holes at the top, with adjustable-length locks connected at both ends. The preset steel cable length limits the U-TENG's deformation response within a safe stretching range. When the umbilical cable is overstretched, the steel cable absorbs the tensile force, preventing U-TENG damage due to excessive deformation. Fatigue damage to umbilical cables is an inherent characteristic, but such damage has minimal impact on sensors that rely on localized tensile excitation. Furthermore, the U-TENG is not fully embedded within the umbilical cable, thus it does not accelerate its fatigue failure process.

In the application scenario of this study, the sensor is mounted externally on the umbilical cable via a bracket. During actual operation, its primary load bearing is axial tensile force, while normal forces and shear forces are relatively minor. Furthermore, these forces are constrained by the structural design of the umbilical cable's outer sheath, rendering their influence significantly less than that of the axial tensile load. Therefore, this study focuses on testing axial tensile performance.

Fig. 2c shows the COMSOL simulation results of the U-TENG under different stretching conditions: (i) static state; (ii) state stretched by 5 cm (50 % strain) state. Specifically, all material parameters used in the simulation are based on the actual physical properties of the experimental materials: the relative permittivity of the silicone rubber (Dragon Skin 00–30) is set to 2.8, and the conductivity of the copper electrodes is set to 5.8×10^7 S/m. Geometric dimensions match those of the fabricated U-TENG, including silicone rubber layer thickness, spiral electrode diameter, and number of turns. Regarding boundary conditions, the electrode surfaces were defined as ideal conductors. The contact interface between the silicone rubber surface and the electrodes was designated as a charge generation region. Corresponding displacement constraints were applied under tensile and bending loading conditions. The simulation results indicate that the U-TENG maintains its overall structural integrity during stretching. Axial deformation occurs with a concurrent reduction in diameter and dielectric layer thickness, following Poisson's effect described by $D = D_o \times (1 - s \times \nu)$, D_o denotes the original diameter, s represents the strain, and ν is the material's transverse contraction coefficient. This relationship quantifies how the diameter changes proportionally with strain, directly influencing the contact area between electrodes.

Fig. 2d illustrates the working principle of the U-TENG in converting tensile force into an electrical signal. In the initial state (Fig. 2d(i)), the intermediate dielectric layer (Dragon Skin 00–30) is in close contact with the electrodes on either side. Due to the difference in electronegativity between the materials, equal and opposite charges are generated at the interface, leaving the system in electrostatic equilibrium with no current output from the external circuit. During stretching, the outer layer (Ecoflex 00–10, Shore hardness 10 C) is softer than the friction layer, leading to more pronounced radial contraction. This changes the distance between the electrodes and the friction layer: one side moves closer to the dielectric layer, while the other moves farther away, disrupting the original equilibrium and generating a potential difference. Under the influence of electrostatic induction, free electrons flow along the external circuit from the near electrode to the far electrode,

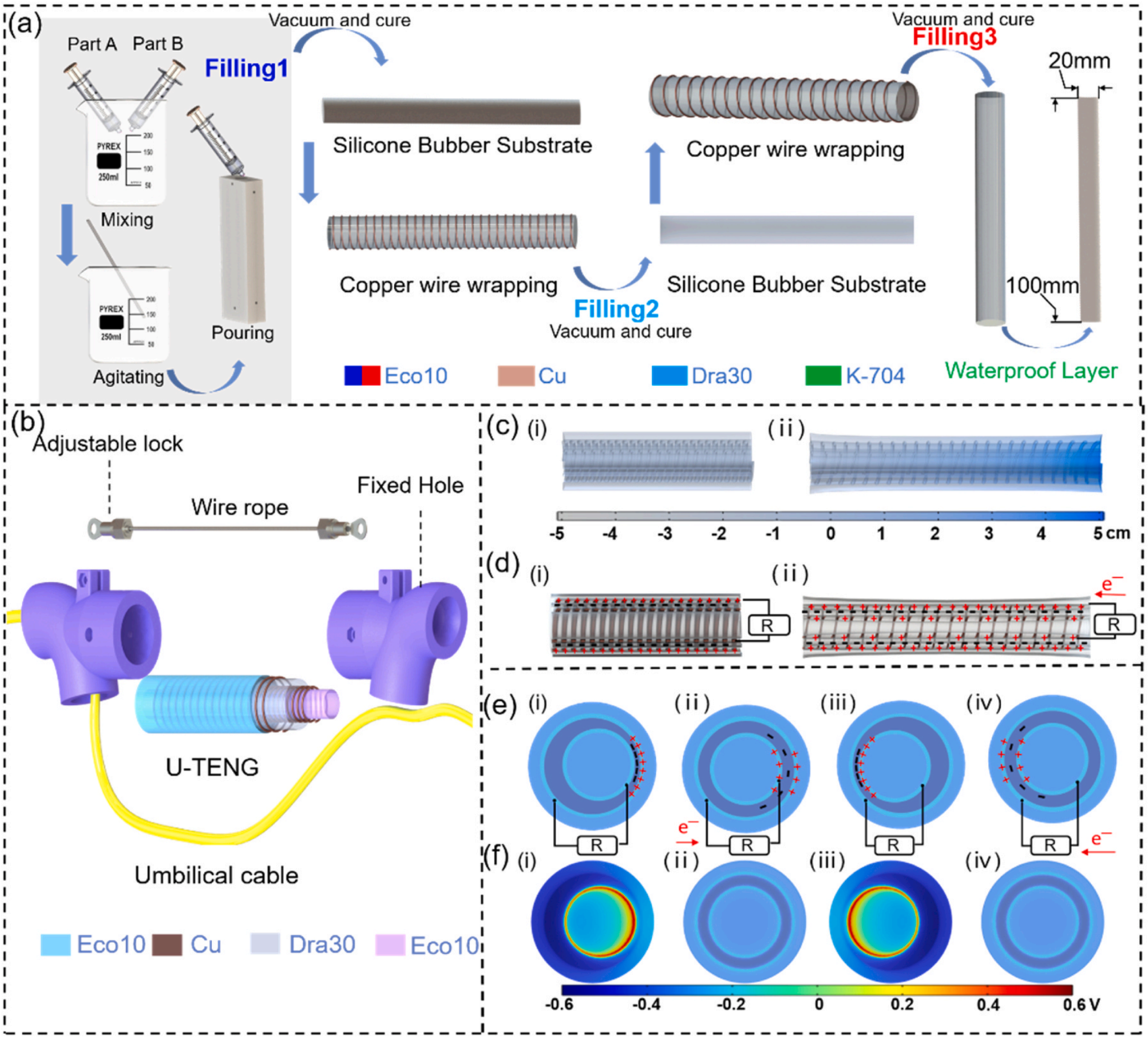

Fig. 2. Structural design and sensing mechanism of the U-TENG. (a) Schematic diagram illustrating the device manufacturing process. (b) Overall structural diagram of the U-TENG. (c)(i)-(c)(ii) COMSOL simulation results for the tensile sensor. (d)(i)-(d)(ii) Charge transfer process in the U-TENG during tensile deformation. (e)(i)-(e)(iv) Charge transfer process in the U-TENG during bending deformation. (f)(i)-(f)(iv) COMSOL simulation of the potential distribution of the U-TENG during bending.

generating an induced current. As shown in Fig. 2d(ii), when the stretch reaches its maximum, the potential difference between the electrodes also reaches its peak, and the output voltage reaches its maximum value. Subsequently, deformation stops, charge redistribution moves toward equilibrium, and the induced current gradually diminishes; when the U-TENG returns to its original state, the electrodes come into contact again, generating a current in the opposite direction and completing a full signal conversion cycle.

The electromechanical conversion principle of the U-TENG under bending excitation is shown in Fig. 2e. It operates in a contact-separation mode during bending, utilizing material electronegativity differences and electrostatic induction for charge transfer. Fig. 2e(i) shows the initial stage of a motion cycle, during which the silicone rubber and electrodes undergo relative movement. Due to bending deformation, the gap on one side between the silicone rubber and the outer electrode decreases, causing the silicone rubber to contact both the inner and outer electrodes. Because of the difference in dielectric properties between the silicone rubber and the electrodes, contact induces electron transfer from the electrodes to the silicone rubber surface. As a result, the silicone surface exhibits a negative charge, while the electrode surface carries an equal positive charge. This electrostatic equilibrium creates a persistent potential distribution. In the second stage (ii), as the U-TENG deformation recovers, the electrostatic equilibrium between the two materials is disrupted. Due to electrostatic induction, some electrons from the outer electrode flow through the external circuit to the inner electrode. When the U-TENG bends to the other side (iii), the gap between the outer electrode on that side and the silicone rubber decreases, causing the transferred electrons to be attracted to the inner electrode due to electrostatic induction. When the U-TENG returns to the original (concentric) position (iv), a portion of electrons is again transferred to the outer electrode under the influence of electrostatic induction.

2.2. *Output performance of U-TENG*

The output characteristics of the sensor depend not only on external stimuli but also on material properties and structural parameters—relationships that can be quantified using core theoretical models derived from its contact-separation working mechanism (detailed in Section 2.1). For the U-TENG, which operates via periodic contact and separation between triboelectric layers, the open-circuit voltage (V_{oc}) and short-circuit transferred charge (Q_{sc}) are governed by Eq. 1 and Eq. **2**.

$$V_{OC} = \frac{\sigma x(t)}{\varepsilon_0}\# \tag{1}$$

$$Q_{SC} = \frac{S\sigma x(t)}{d_0 + x(t)}\# \tag{2}$$

Here, σ denotes the surface charge density of the dielectric layer (a material-dependent property), $x(t)$ is the dynamic separation distance between the friction layers during deformation, $\varepsilon_0$is the vacuum permittivity, S represents the effective contact area, and d_0 is the dielectric layer thickness. These equations reveal that V_{oc} and Q_{sc} are directly influenced by the dielectric layer's material properties (via σ) and thickness (via d_0), highlighting the need to optimize these parameters to enhanced performance.

To validate these theoretical relationships and identify optimal parameters, a U-TENG testing platform was established (Fig. 3a), with motor parameters adjusted to simulate various excitation conditions. A high-resistance electrometer was used to measure real-time V_{oc} and Q_{sc} signals.

As the core component responsible for charge accumulation and transfer, the dielectric layer greatly influences signal stability. Five silicone materials were selected in ascending order of elastic modulus and hardness: Ecoflex 00–10, Ecoflex 00–20, Ecoflex 00–30, Dragon Skin 00–20, and Dragon Skin 00–30. As shown in Fig. 3b, under stretching conditions of 1.0 Hz and 20 % strain (corresponding to a 2 cm extension), the sensor with a Dragon Skin 00–30 dielectric layer exhibited the best performance, with a V_{oc} of 7.57 V and a Q_{sc} of 2.12 nC. These represent increases of 145 % and 409 %, respectively, compared to Ecoflex 00–10. This improvement is primarily attributed to the higher tear strength and elastic modulus of Dragon Skin 00–30, which help maintain stable contact during stretching and reduce charge loss.

Due to spatial constraints for embedding the sensor within the umbilical cable, dielectric layer thicknesses ranging from 0.5 mm to 2.5 mm were tested to evaluate their impact on output performance. As shown in Fig. 3c, at 1.0 Hz and 10 % strain, the 2.5 mm thick dielectric layer produced V_{oc} and Q_{sc} values of 2.34 V and 7.48 nC, respectively—significantly higher than those of the 0.5 mm thickness (V_{oc}: 1.08 V; Q_{sc}: 3.07 nC). As illustrated in Fig. 3d, Voc exhibits a significant linear relationship with the dielectric layer thickness, following $U = 0.7157d + 0.6771$ — where d represents the dielectric layer thickness and U denotes the output voltage. The coefficient of determination (R^2) is 0.93796, with a maximum deviation of only 0.21 %. Consequently, a dielectric layer thickness of 2.5 mm was selected as the optimal structural parameter for the U-TENG.

In practical applications, umbilical cables are subjected to repeated

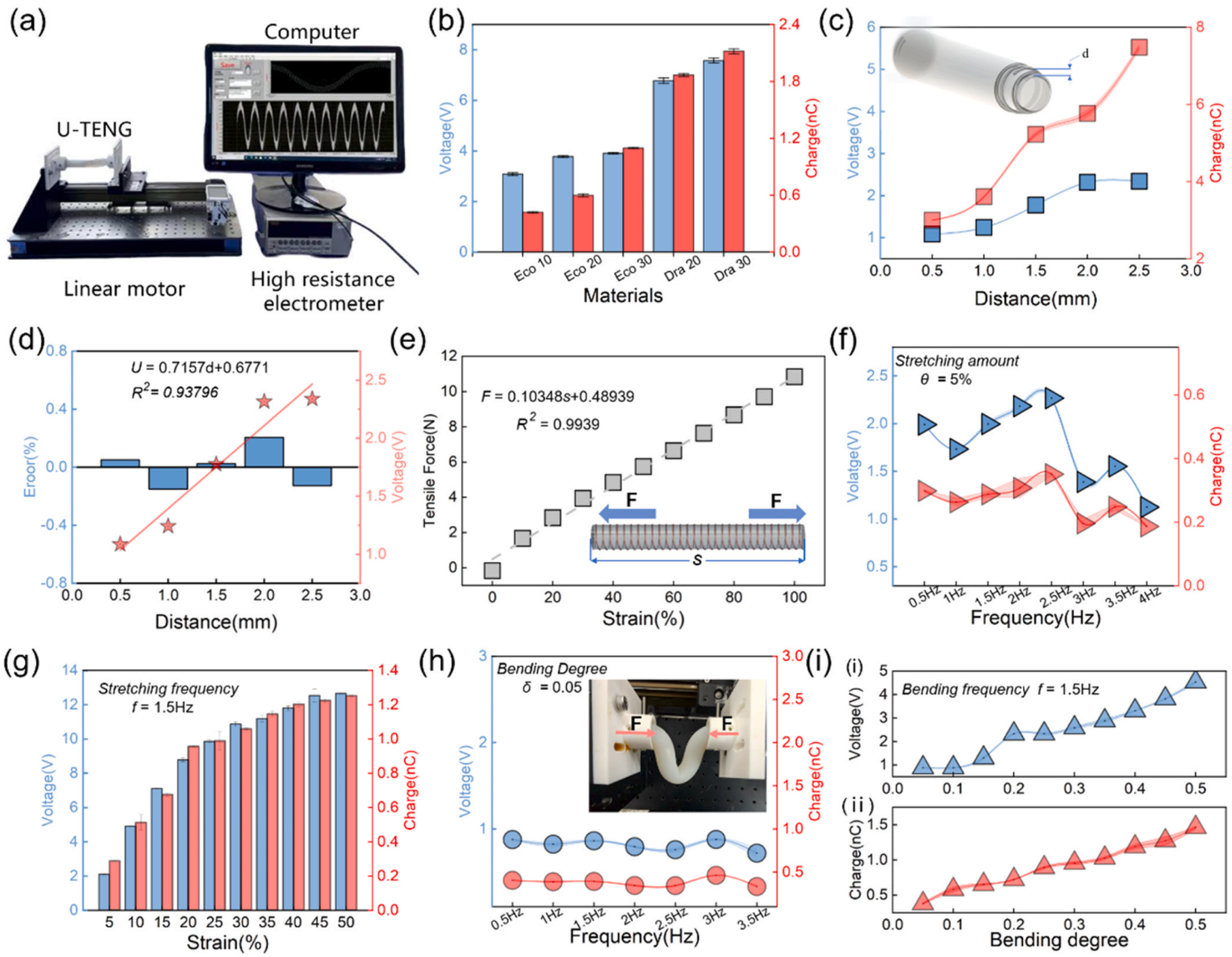

Fig. 3. Output performance of U-TENG. (a) Schematic diagram of the experimental setup. (b) Influence of dielectric material on sensor output performance. (c) Influence of dielectric layer thickness on sensor output performance. (d) Fitted linear relationship between V_{oc} and dielectric layer thickness. (e) Fitted linear relationship between tensile force and strain. (f) Influence of stretching frequency on sensor output performance. (g) Influence of tensile strain on sensor output performance. (h) Influence of bending frequency on sensor output performance. (i) Influence of bending degree on sensor output performance.

stretching over extended periods, requiring sensors with stable mechanical properties. To verify the consistency of tensile responses, 20 repeated tensile tests were conducted over a range of strain levels. As shown in Fig. 3e, within the strain range up to 100 %, there is a strong linear correlation between strain and tensile force, which is well-described by $F = 0.10348s + 0.48939$, where F is the tensile force and s represents the strain. This linear relationship, characterized by a high coefficient of determination (R^2) of 0.9939 and a maximum deviation of only 0.27 %, confirms the U-TENG's reliable performance in quantifying tensile forces across the tested strain range. Notably, when the strain reaches 100 %, the U-TENG still exhibits a stable response.

Due to variations in stretching frequency during practical applications, this study evaluated the sensor's response to different frequencies under a fixed 5 % strain condition. Stretching was periodically applied at frequencies ranging from 0.5 Hz to 4.0 Hz, with 0.5 Hz as the incremental interval. Since silicone rubber exhibits varying degrees of recovery at different stretching rates, the U-TENG voltage output did not show a clear linear trend with frequency (Fig. 3f). Fig. S1 (Supporting Information) further demonstrates the U-TENG's output waveform, confirming accurate synchronization with stimuli at varying frequencies. To clarify the effect of strain on output performance, the sensor's responses were measured as strain increased from 5 % to 50 % at a fixed frequency of 1.5 Hz. V_{oc} increased from 2.13 V to 12.67 V, and Q_{sc} from 0.29 nC to 1.25 nC (Fig. 3g). Furthermore, this work investigated the performance output when the strain was increased from 5 % to 50 % at different strain frequencies. As shown in Fig. S2, output voltage amplitude of the U-TENG increases significantly with the strain, but there is no obvious correlation with the frequency. Thus, the U-TENG reliably responds to periodic strain stimuli at various frequencies, with output amplitude primarily determined by strain, demonstrating excellent dynamic stability.

In this work, $\delta = \Delta S/L$, where δ represents the degree of bending and is a dimensionless parameter, ΔS denotes the bending displacement length, and L is the effective length of the sensor. To distinguish between umbilical cable states (stretching versus bending), the U-TENG's response under bending was evaluated. At a fixed bending degree of 0.05 and with periodic excitation frequencies ranging from 0.5 Hz to 3.5 Hz, V_{oc} remained stable around 0.80 V, and Q_{sc} at around 0.40 nC, indicating insensitivity to changes in bending frequency (Fig. 3h). This is because deformation exhibits asymmetric characteristics under bending loads. Compression on one side of the sensor reduces the local gap, while tension on the opposite side increases it. This asymmetric contact-separation process disrupts the symmetry of charge distribution. Consequently, the output signal is highly sensitive to curvature but remains largely unaffected by bending frequency. This supports effective differentiation between stretching and bending signals. Fig. S3 confirms good synchronization and periodic response under varying bending frequencies.

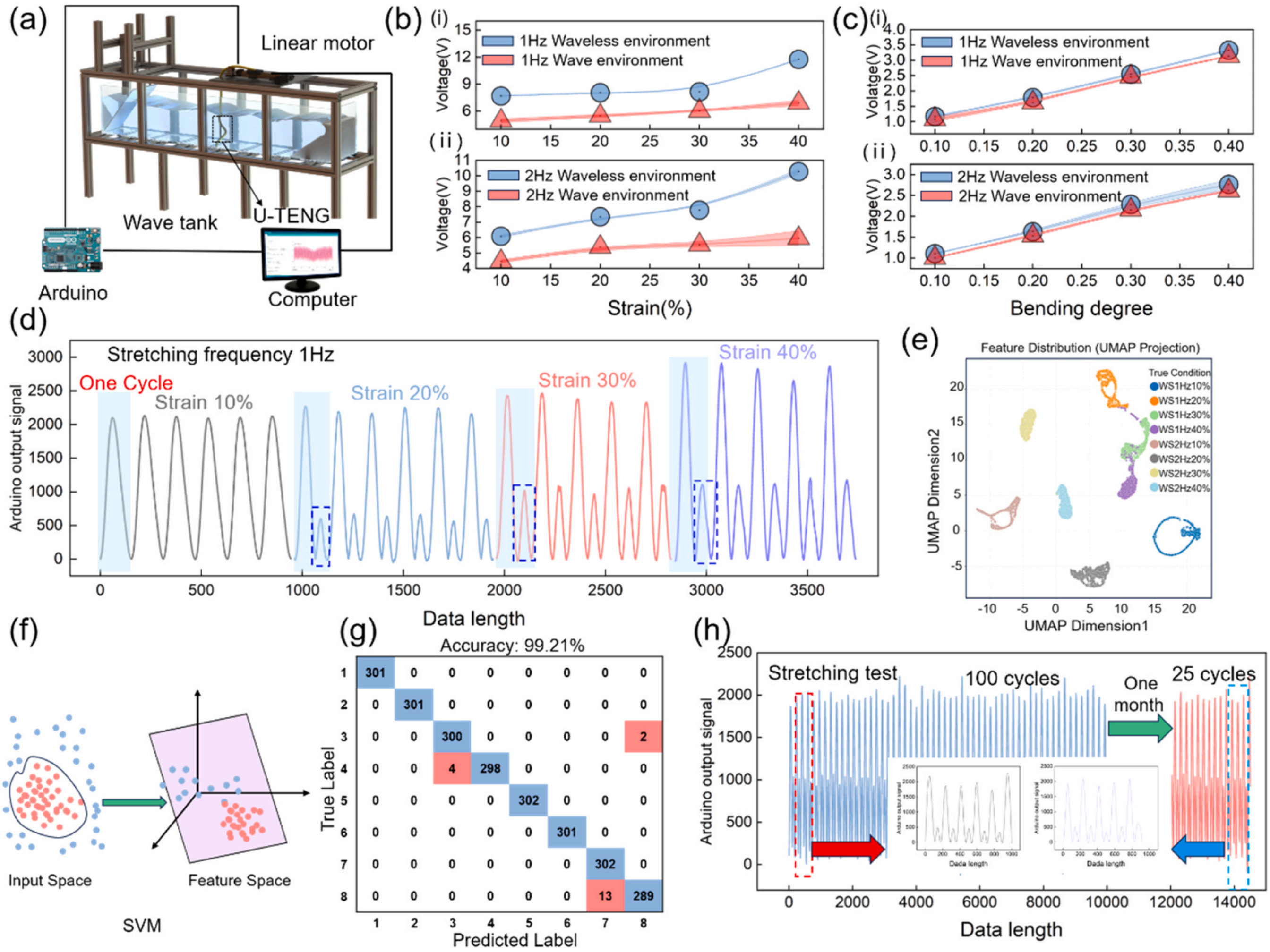

True Label \ Predicted Label	1	2	3	4	5	6	7	8
1	301	0	0	0	0	0	0	0
2	0	301	0	0	0	0	0	0
3	0	0	300	0	0	0	0	2
4	0	0	4	298	0	0	0	0
5	0	0	0	0	302	0	0	0
6	0	0	0	0	0	301	0	0
7	0	0	0	0	0	0	302	0
8	0	0	0	0	0	0	13	289

Fig. 4. Sensor output performance and signal processing in underwater environments. (a) Schematic diagram of the experimental setup. (b)(i) – (b)(ii) Influence of wave motion on sensor output performance in the stretched state. (c)(i)–(c)(ii) Influence of wave motion on sensor output performance in the bending state. (d) Modulation voltage waveforms at different strain under a 1 Hz strain frequency in a wave environment. (e) Dimension reduction visualization of data from eight strain states. (f) Schematic diagram of the SVM algorithm. (g) Confusion matrix for eight strain states (accuracy: 99.21 %). (h) Sensor durability test diagram.

Finally, the effect of bending degree on output was tested at a bending frequency of 1.5 Hz. V_{oc} increased from 0.88 V to 4.54 V, and Q_{sc} from 0.38 nC to 1.46 nC, demonstrating high sensitivity to bending degree (Fig. 3i). Fig. S4 further verifies this relationship. Therefore, the U-TENG not only stably responds to bending frequencies but also effectively reflects bending magnitude through output amplitude, enabling clear distinction between stretching and bending signals.

2.3. USV-ROV cable condition monitoring

Given that ROVs typically operate in low-frequency wave environments, ensuring stable underwater sensor output is crucial. This study established an underwater testing platform (Fig. 4a), consisting of a wave-generating tank (2400 × 400 × 400 mm), a linear motor, an Arduino MEGA microcontroller, and a host computer. The platform has overall dimensions of 2635 × 600 × 1115 mm. During experiments, the U-TENG was fixed to one end of the umbilical cable and placed at the tank bottom. Tensile and bending stimuli were applied by the linear motor positioned above the tank. A fixed pulley stabilized displacement transmission, ensuring accurate displacement transfer. Testing was conducted under typical wave conditions (15 cm wave height and 0.5 Hz frequency) to simulate real sea conditions.

To evaluate the U-TENG's output performance under wave interference, the tensile response was tested first. As shown in Fig. 4b(i) and (ii), at stretching frequencies of 1.0 Hz and 2.0 Hz, the U-TENG's V_{oc} increased steadily with strain, regardless of wave presence. The wave environment resulted in an average reduction in V_{oc} of approximately 3.08 V (1.0 Hz) and 1.97 V (2.0 Hz), but the correlation between strain and output amplitude remained statistically significant.

Subsequently, the response under bending stimulation was tested. As shown in Fig. 4c, V_{oc} increases as the bending degree increases from 0.1 to 0.5. Although the waves caused the output amplitude to decrease by approximately 0.133 V (1 Hz) and 0.121 V (2 Hz) (Fig. 4c(i) and (ii)), the overall trend of the bending response remained unaffected. Despite wave-induced interference on output amplitude, the U-TENG still maintains a stable output. Notably, comparing the stretching and bending signals reveals that the output characteristics under these two excitation types—such as amplitude variation range and frequency sensitivity—differ significantly, laying the foundation for accurately distinguishing between the two deformation types.

To facilitate integration into unmanned boat platforms with limited space and power supply, this work selected the Arduino MEGA as the signal acquisition module, owing to its small size, low power consumption, and stable performance. Its built-in Analog-to-Digital Converter (ADC) enables real-time signal acquisition, which, combined with filtering algorithms, effectively suppresses environmental noise. It also incorporates a dynamic baseline tracking mechanism to correct baseline drift and low-frequency interference in real time, ensuring signal stability. Fig. S5 validates the reliability and practicality of this approach, and subsequent analyses all use the Arduino output modulated voltage signals processed by the Arduino MEGA. These Arduino output signals align with the trends of the original signals and accurately reflect the U-TENG's dynamic response and characteristics (such as response onset, peak, and rebound fluctuations), thereby facilitating subsequent signal analysis.

Fig. 4d shows the modulated voltage waveforms at different strain measured by Arduino Mega at a strain frequency of 1.0 Hz in a sea wave environment. The light blue region represents the U-TENG response during a single stretch cycle: initial voltage is near zero, and as stretching progresses, the voltage gradually increases, peaking at maximum stretch. When the device returns to its original state, the voltage gradually decreases to zero. The blue-purple region in the figure indicates the rebound signal after stretching ends. This rebound occurs due to the high elastic modulus of silicone rubber: the release of elastic potential energy after stretching causes a brief reverse rebound. The rebound amplitude increases with the stretching rate. Within the 10–40 % stretch range, both the main peak and rebound characteristics increase with the stretching rate. The waveform features under different operating conditions are clearly distinguishable, providing an effective basis for machine learning classification.

To assess data separability under different operating conditions, multidimensional features were extracted from the original strain signals, and the Uniform Manifold Approximation and Projection (UMAP) algorithm was used for dimensionality reduction and visualization. As shown in Fig. 4e, the dimensionally reduced samples form distinct clusters in two-dimensional space, indicating good separability among the strain states and supporting the development of subsequent classification models. Fig. S6 and S7 further compare the waveforms of signals with different bending degrees and strain levels under 1.0 Hz excitation in a wave environment, along with dimensionality reduction visualizations of data from all operating conditions. The results show significant differences between the two types of signals in waveform, amplitude, and distribution within the feature space, verifying the feasibility of classification.

To efficiently classify umbilical cable stress response signals under wave disturbances, this study adopted Support Vector Machines (SVM) as the core classification algorithm. Compared to neural networks, SVM exhibits better generalization ability and faster convergence with small sample sizes. Fig. 4f illustrates the schematic diagram of the SVM. Specifically, time-domain signals of modulated voltage were collected under wave frequencies of 1 Hz and 2 Hz, with combinations of different strain levels (10 %, 20 %, 30 %, 40 %) resulting in eight operating conditions. Each dataset contained 60,000 sampling points. After preprocessing with sliding window segmentation (400 points in length, 80 % overlap rate) and data normalization, time-domain features were extracted to construct the dataset. We employed an SVM model with a radial basis function (RBF) kernel, optimizing performance through adaptive adjustment of the γ parameter and category weighting strategy. The dataset was split into 75 % for training and 25 % for testing. As shown in Fig. 4g, the model achieved a classification accuracy of 99.21 % on the test set. Fig. S8 further demonstrates that the accuracy for 16 types of strain conditions under bending and stretching scenarios reached 97.18 %, validating the efficiency and reliability of SVM in umbilical cable state recognition. Fig. S9, S10**, and S11** demonstrate the accuracy rates of the 1D Convolutional Neural Network (1DCNN) algorithm on the tensile, bending, and combined tensile-bending test sets, which are 99.39 %, 89.02 %, and 95.84 %, respectively.

Finally, the underwater durability of the U-TENG was evaluated. As shown in Fig. 4h, After one month of underwater immersion, the U-TENG underwent repeated stretching tests in a wave environment. Its modulation voltage stabilized around 2000, and the output waveform exhibited good periodicity with no significant degradation, demonstrating long-term durability and reliability in dynamic operating conditions such as ROV umbilical cables. Fig. S12 shows the one-month underwater bending endurance test of U-TENG. The Arduino output signal remained stable around 500 before and after the test, verifying that U-TENG maintains excellent output stability even under repeated bending conditions.

3. Application demonstration

To validate the sensor's perception capabilities, this study established a USV-ROV collaborative testing platform Fig. 5a(i), comprising a USV (1.5 × 0.5 × 0.7 m), an ROV, and a sensor system. Fig. 5a(ii) further details the ROV and sensor system. The USV is equipped with an Arduino MEGA for sensor data acquisition and an STM32F103 microcontroller to control the winch for deploying and retrieving the umbilical cable. The winch before modification only supported three manual switch settings: forward, stop, and reverse, and could not continuously adjust the speed. To enable automated control, this study integrated a 5 V MG90S servo motor via a connector, with its angle controlling the winch's movements.

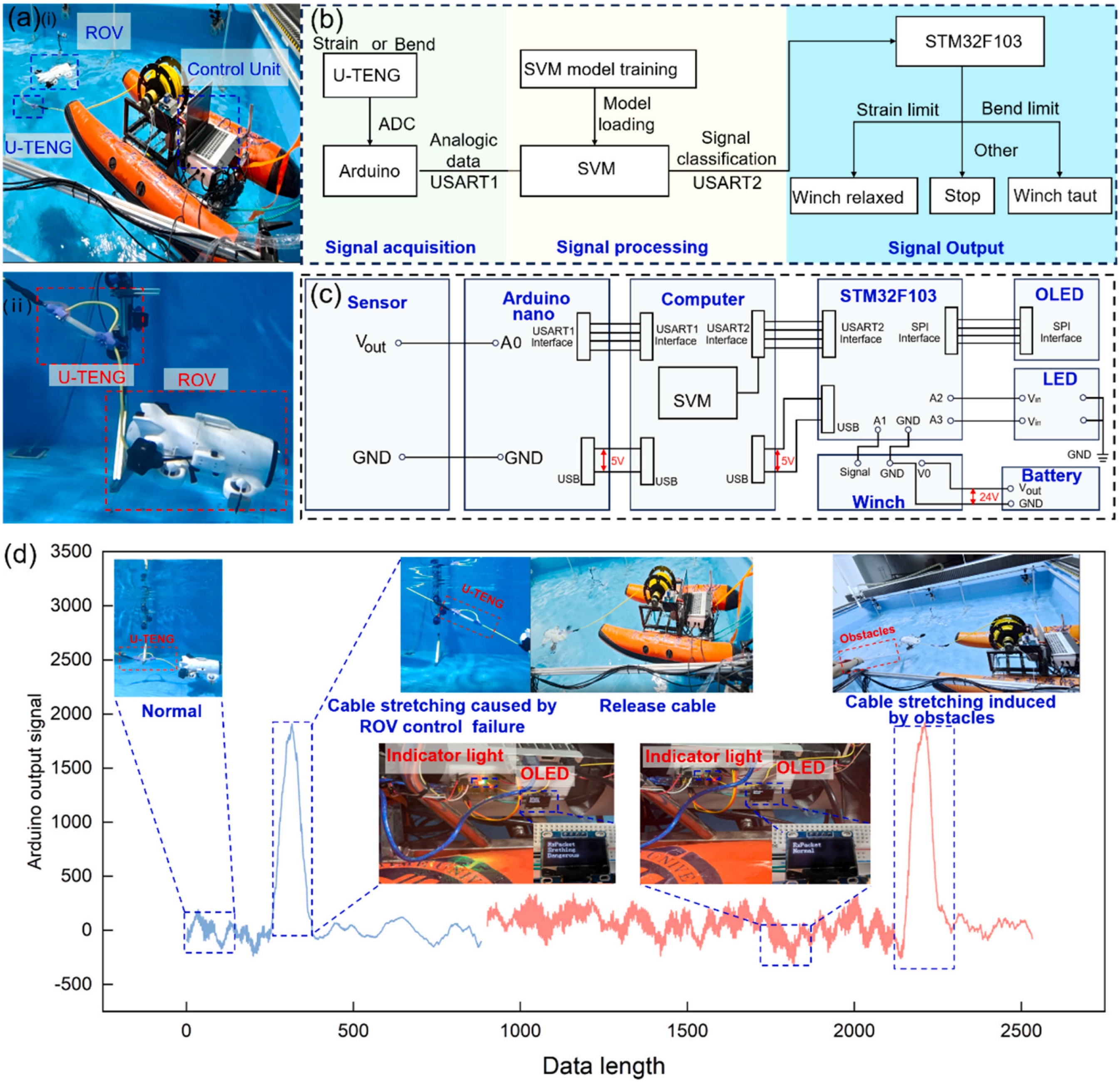

Fig. 5. Application of sensors on the USV-ROV platform. (a) (i) Schematic diagram of the experimental setup. (a) (ii) Details of the U-TENG and ROV. (b) Flowchart of signal acquisition and processing algorithms. (c) Schematic diagram of system circuit connections. (d) Sensor output signal when the umbilical cable is overstretched.

Fig. 5b illustrates the overall process of the friction-based sensor signal acquisition and processing system implemented on the Arduino MEGA. The system integrates the host computer's real-time processing capabilities with the microcontroller's executive control, enabling identification and control of the umbilical cable's condition. The control process involves three primary stages: first, during signal acquisition, the Arduino MEGA continuously collects sensor signals via the ADC module, applies basic signal conditioning, and transmits the data to the host computer through the USART1 serial port; second, during signal processing, the host computer receives the data, loads the pre-trained SVM model, classifies the signals, and sends the results to the STM32F103 via the USART2 serial port; third, during signal response, the STM32F103 makes decisions based on the classification results: if the cable is identified as "stretching" or "bending" with amplitude within the normal range, no action is taken. If identified as "excessive stretching" or "excessive bending," the winch is controlled to tighten or loosen accordingly, achieving adaptive regulation of the cable tension.

The system circuit connection diagram is shown in Fig. 5c. The winch is powered by a 24 V lithium battery, and its ground line (GND, ground) must share a common ground with the control circuit to ensure signal consistency. The winch servo is controlled by Pulse Width Modulation (PWM) pulses with a 20 ms period; the pulse width ranges from 0.5 ms to 2.5 ms, corresponding to servo angles from 0° to 180°. Specifically, 0.5 ms corresponds to 0° (winch forward rotation), 1.5 ms to 90° (winch stopped), and 2.5 ms to 180° (winch reverse rotation). The actual circuit connection is shown in Fig. S13.

Fig. 5d shows the U-TENG voltage responses corresponding to the umbilical cable status of the ROV under different operating conditions.

To enhance system operability, this study also designed a visualization alarm module that provides visual alerts through indicator lights, assisting operators in responding promptly. Under normal conditions ("Normal"), the cable is slack, the U-TENG outputs low-level noise, and the voltage is near the baseline; the system remains stationary, the indicator light is off, and the OLED display reads "Normal". When abnormalities in ROV control pull the cable taut, the sensor voltage increases significantly. Upon detection, the system automatically controls the winch to release the cable, the indicator light stays on, and the OLED display switches to "Stretching Dangerous". Details can be found in Supporting Information Movie S1 **(Part 1).** During retrieval, if an obstacle obstructs the cable and causes it to stretch again, the system pauses winch retrieval and resumes operation once tension decreases. Details can be found in Movie S1 **(Part 2).** The results indicate that the system can effectively identify the umbilical cable's condition under various operating conditions and trigger corresponding adaptive adjustments and real-time alarms, thereby significantly enhancing the ROV's safety and operability in complex operational environments.

4. Conclusion

As a core component in the USV-ROV collaborative system, the umbilical cable is of great significance but confronted with destruction due to excessive stretching. To address this issue, a machine learning-driven triboelectric nanogenerator (U-TENG) for self-powered condition monitoring and regulation of the USV-ROV umbilical cable is firstly proposed. The U-TENG is securely mounted on the umbilical cable via a bracket without affecting its original mechanical properties. The strain rate shows a linear relationship with R^2 of 0.9929 corresponding to the stretching force within 0–100 % elastic region, which thanks to the stretchability of the silicone rubber and helix electrodes. Furthermore, the effectiveness of the U-TENG is verified in the wave tank with a wave height of 15 cm and frequency of 0.5 Hz. To further investigate the underwater cable condition sensing, analysis was performed under different bending states in the wave tank. Moreover, a machine learning-based model is proposed based on the sensing data of the U-TENG, cable condition identification accuracy of 97.18 % is achieved under 16 different combinations of stretching and bending states. It is worth mentioning that an identification accuracy of 99.21 % is accomplished under 8 different stretching states. Moreover, an integrated system for umbilical cable state monitoring and adaptive control was constructed based on the machine-learning enabled U-TENG, which is composed of a USV, a ROV, and a cable regulation winch on the USV. Finally, the integrated system successfully recognizes the umbilical cable state in real time and achieves automatic umbilical cable tension control by controlling the winch in the water tank. Overall, it shows that the proposed machine-learning based U-TENG is able to achieve real-time sensing, accurate identification, and adaptive regulation of the USV-ROV umbilical cable, which provides a new solution for umbilical cable state monitoring. To drive this technology from the laboratory to engineering applications, our future work will focus on long-term reliability verification in real marine environments, sustained biofouling studies, and the miniaturization of electronic components. We believe this technology will achieve breakthrough progress in the future.

CRediT authorship contribution statement

Yan Yang: Writing – review & editing, Writing – original draft, Software, Investigation, Data curation. **XU MINYI:** Supervision, Funding acquisition. **Xingjia Jiang:** Validation, Resources, Methodology, Formal analysis. **Fangyang Dong:** Formal analysis. **Hengxu Du:** Data curation. **Taili Du:** Writing – review & editing, Supervision, Project administration. **Qiang Zhao:** Resources, Methodology. **Mengwei Wu:** Supervision, Project administration.

Declaration of Competing Interest

The authors declare that they have no known competing financial interests or personal relationships that could have appeared to influence the work reported in this paper.

Acknowledgements

The work is supported by the Basic Research Project of the Liaoning Provincial Department of Education (LJ212510151019), the China Postdoctoral Science Foundation (Grant No. 2025T180074, 2024M750297), Scientific Research Innovation Capability Support Project for Young Faculty (Grant No. ZYGXQNJSKYCXNLZCXM O1P), Beijing Key Laboratory of High-Entropy Energy materials and Devices, Beijing Institute of Nanoenergy and Nanosystems (No. GS2025MS004), the Jilin Provincial Department of Education Outstanding Youth Fund (Grant No. JJKH20240038KJ).

Appendix A. Supporting information

Supplementary data associated with this article can be found in the online version at doi:10.1016/j.sna.2025.117134.

Data availability

Data will be made available on request.

References

[1] F. Zhang, O. Ennasr, E. Litchman, X. Tan, Autonomous sampling of water columns using gliding robotic fish: algorithms and Harmful-Algae-Sampling experiments, IEEE Syst. J. 10 (2016) 1271–1281, https://doi.org/10.1109/JSYST.2015.2458173.

[2] B. Lyu, Z. Zeng, D. Lu, L. Lian, J. Tu, L. Xiao, Y. Liu, Combined Small-Sized USV and ROV observation system for Long-Term, Large-Scale, spatially explicit aquatic monitoring, in: OCEANS - MTSIEEE Kobe Techno-Oceans OTO, IEEE, Kobe, 2018, 2018, pp. 1–6, https://doi.org/10.1109/OCEANSKOBE.2018.8559206.

[3] A.S. Gower, Offshore integrity management and life extension - a vision of the application of subsea robotics in assuring asset integrity, OnePetro (2023), https://doi.org/10.4043/32198-MS.

[4] M.C. Fagot, S.E. Spychalski, Deep-Towed Array Geophysical System (DTAGS): A Hardware Description, (1984). ⟨https://apps.dtic.mil/sti/html/tr/ADA142970/⟩ (accessed July 28, 2025).

[5] A. Lasbouygues, S. Louis, B. Ropars, L. Rossi, H. Jourde, H. Delas, P. Balordi, R. Bouchard, M. Dighouth, M. Dugrenot, E. Jacquemin, F. Vasseur, L. Lapierre, D. Andreu, Robotic mapping of a karst aquifer ⋆, (n.d.).

[6] The Tension Calculation of Self-Propelled, Cable-Controlled Vehicles' Cables | Scientific.Net, (n.d.). ⟨https://www.scientific.net/AMR.823.24⟩ (accessed July 28, 2025).

[7] A. Reda, J. Thiedeman, M.A. Elgazzar, M.A. Shahin, I.A. Sultan, K.K. McKee, Design of subsea cables/umbilicals for in-service abrasion - part 1: case studies, Ocean Eng. 234 (2021) 108895, https://doi.org/10.1016/j.oceaneng.2021.108895.

[8] C. Viel, Self-Management of ROV umbilical using sliding buoys and stop, IEEE Robot. Autom. Lett. 7 (2022) 8061–8068, https://doi.org/10.1109/LRA.2022.3187267.

[9] T.Z. Htun, H. Suzuki, D. García-Vallejo, On the theory and application of absolute coordinates-based multibody modelling of the rigid–flexible coupled dynamics of a deep-sea ROV-TMS (tether management system) integrated model, Ocean Eng. 258 (2022) 111748, https://doi.org/10.1016/j.oceaneng.2022.111748.

[10] B.A. Abel, Underwater Vehicle tether management systems, in: Proc. Ocean., IEEE, Brest, France, 1994: p. II/495-II/500. https://doi.org/10.1109/OCEANS.1994.364094.

[11] M. Laranjeira, C. Dune, V. Hugel, Catenary-based visual servoing for tether shape control between underwater vehicles, Ocean Eng. 200 (2020) 107018, https://doi.org/10.1016/j.oceaneng.2020.107018.

[12] M.T. Vu, H.-S. Choi, T.Q.M. Nhat, D.-H. Ji, H.-J. Son, Study on the dynamic behaviors of an USV with a ROV, OCEANS 2017 Anchorage (2017) 1–7. ⟨https://ieeexplore.ieee.org/abstract/document/8232137⟩ (accessed July 28, 2025).

[13] T.Z. Htun, H. Suzuki, D. García-Vallejo, Dynamic modeling of a radially multilayered tether cable for a remotely-operated underwater vehicle (ROV) based on the absolute nodal coordinate formulation (ANCF), Mech. Mach. Theory 153 (2020) 103961, https://doi.org/10.1016/j.mechmachtheory.2020.103961.

[14] P. Chen, Y. Liu, S. Yang, J. Chen, Q. Zhang, Y. Tang, Dynamic characteristics of deep-sea ROV umbilical cables under complex sea conditions, Ocean Eng. 239 (2021) 109854, https://doi.org/10.1016/j.oceaneng.2021.109854.

[15] S.M. Hong, K.N. Ha, J.-Y. Kim, Dynamics modeling and motion simulation of USV/UUV with linked underwater cable, J. Mar. Sci. Eng. 8 (2020) 318, https://doi.org/10.3390/jmse8050318.

[16] O. Tortorici, C. Anthierens, V. Hugel, A new Flex-Sensor-Based Umbilical-Length management system for underwater robots, in: Eur. Conf. Mob. Robots ECMR, 2023, IEEE, Coimbra, Portugal, 2023, pp. 1–6, https://doi.org/10.1109/ECMR59166.2023.10256299.

[17] H. Huang, Q. Tang, Y. Li, L. Wan, Y. Pang, Dynamic control and disturbance estimation of 3D path following for the observation class underwater remotely operated vehicle, Adv. Mech. Eng. 5 (2013) 604393, https://doi.org/10.1155/2013/604393.

[18] C. Viel, Self-Management of ROV Umbilical using sliding element: a general 3D-model - Full version, (2023). ⟨https://hal.science/hal-04157011⟩ (accessed July 28, 2025).

[19] C. Zhao, T. Du, B. Ge, Z. Xi, Z. Qian, Y. Wang, J. Wang, F. Dong, D. Shen, Z. Zhan, M. Xu, Coaxial flexible Fiber-Shaped triboelectric nanogenerator assisted by deep learning for Self-Powered vibration monitoring, Small 20 (2024) 2307680, https://doi.org/10.1002/smll.202307680.

[20] J. Liu, B. Liu, Z. Xi, H. Yang, Y. Li, H. Du, Z. Mu, J. Si, S. Wang, P. Xu, M. Xu, Highly sensitive and integratable triboelectric bionic lateral line sensor for flow recognition of underwater vehicle, Adv. Mater. Technol. 10 (2025) 2500072, https://doi.org/10.1002/admt.202500072.

[21] W. Sun, TENG-Bot: triboelectric nanogenerator powered soft robot made of uni-directional dielectric elastomer, Nano Energy (2021).

[22] K. Xia, M. Yu, Y. Luo, Y. Ding, All-foam intrinsic triboelectric static and dynamic pressure sensor with a standardized DC/AC measurement method for industrial robots, Nano Energy 139 (2025) 110953, https://doi.org/10.1016/j.nanoen.2025.110953.

[23] B. Liu, B. Dong, H. Jin, P. Zhu, Z. Mu, Y. Li, J. Liu, Z. Meng, X. Zhou, P. Xu, M. Xu, Deep-Learning-Assisted triboelectric whisker sensor array for Real-Time motion sensing of unmanned underwater vehicle, Adv. Mater. Technol. 10 (2025) 2401053, https://doi.org/10.1002/admt.202401053.

[24] J. Xu, A triboelectric multifunctional sensor based on the controlled buckling structure for motion monitoring and bionic tactile of soft robots, Nano Energy (2022).

[25] S. Liu, Triboelectric nanogenerators enabled sensing and actuation for robotics, (2019).

[26] K. Wang, Y. Liu, X. Guan, Z. Wang, Z. Pan, Y. Yu, Y. Yao, T. Li, Ultra-Wideband Detection-Enabled modularized Three-Axis vibration sensor for UAV blade damage monitoring via deep learning, IEEE Trans. Ind. Electron (2025) 1–11, https://doi.org/10.1109/TIE.2025.3561854.

[27] J. Liu, P. Xu, B. Liu, Z. Xi, Y. Li, L. Guo, T. Guan, P. Zhu, Z. Meng, S. Wang, H. Wang, M. Xu, Underwater biomimetic lateral line sensor based on triboelectric nanogenerator for dynamic pressure monitoring and trajectory perception, Small 20 (2024) 2308491, https://doi.org/10.1002/smll.202308491.

[28] K. Dong, X. Peng, J. An, A.C. Wang, J. Luo, B. Sun, J. Wang, Z.L. Wang, Shape adaptable and highly resilient 3D braided triboelectric nanogenerators as e-textiles for power and sensing, Nat. Commun. 11 (2020) 2868, https://doi.org/10.1038/s41467-020-16642-6.

[29] Y. Liu, H. Li, X. Liang, H. Deng, X. Zhang, H. Heidari, R. Ghannam, X. Zhang, Speech recognition using intelligent piezoresistive sensor based on polystyrene sphere microstructures, Adv. Intell. Syst. 5 (2023) 2200427, https://doi.org/10.1002/aisy.202200427.

[30] S. Ji, Three-dimensional skin-type triboelectric nanogenerator for detection of two-axis robotic-arm collision, Nano Energy (2022).

[31] F. Yi, Z. Zhang, Z. Kang, Q. Liao, Y. Zhang, Recent advances in triboelectric Nanogenerator-Based health monitoring, Adv. Funct. Mater. (2019).

[32] K. Xia, Z. Zhu, H. Zhang, C. Du, R. Wang, Z. Xu, Cost-effective triboelectric nanogenerator based on teflon tape and conductive copper foil tape, Microelectron. Eng. 199 (2018) 114–117, https://doi.org/10.1016/j.mee.2018.08.002.

[33] J. Zhu, M. Zhu, Q. Shi, F. Wen, L. Liu, B. Dong, A. Haroun, Y. Yang, P. Vachon, X. Guo, T. He, C. Lee, Progress in TENG technology—A journey from energy harvesting to nanoenergy and nanosystem, EcoMat 2 (2020) e12058, https://doi.org/10.1002/eom2.12058.

[34] Y. Feng, L. Zhang, Y. Zheng, D. Wang, F. Zhou, W. Liu, Leaves based triboelectric nanogenerator (TENG) and TENG tree for wind energy harvesting, Nano Energy 55 (2019) 260–268, https://doi.org/10.1016/j.nanoen.2018.10.075.

[35] M. Li, Z. Li, X. Ye, W. He, L. Qu, M. Tian, A smart Self-Powered rope for Water/Fire rescue, Adv. Funct. Mater. 33 (2023) 2210111, https://doi.org/10.1002/adfm.202210111.

[36] F. Dong, M. Zhu, Y. Wang, Z. Chen, Y. Dai, Z. Xi, T. Du, M. Xu, AI-enabled rolling triboelectric nanogenerator for bearing wear diagnosis aiming at digital twin application, Nano Energy 134 (2025) 110550, https://doi.org/10.1016/j.nanoen.2024.110550.

[37] Y. Zhang, Y. Li, R. Cheng, S. Shen, J. Yi, X. Peng, C. Ning, K. Dong, Z.L. Wang, Underwater monitoring networks based on Cable-Structured triboelectric nanogenerators, Research 2022 (2022) 2022/9809406, https://doi.org/10.34133/2022/9809406.

[38] Biomimetic bimodal haptic perception using triboelectric effect | Science Advances, (n.d.). ⟨https://www.science.org/doi/full/10.1126/sciadv.ado6793⟩ (accessed July 28, 2025).

[39] Triboelectric Nanogenerators as New Energy Technology for Self-Powered Systems and as Active Mechanical and Chemical Sensors | ACS Nano, (n.d.). ⟨https://pubs.acs.org/doi/abs/10.1021/nn404614z⟩ (accessed July 28, 2025).

[40] Flexible triboelectric generator, Nano Energy 1 (2012) 328–334. https://doi.org/10.1016/j.nanoen.2012.01.004.

[41] Y. Pang, T. He, S. Liu, X. Zhu, C. Lee, Triboelectric Nanogenerator-Enabled digital twins in civil engineering infrastructure 4.0: a comprehensive review, Adv. Sci. 11 (2024) 2306574, https://doi.org/10.1002/advs.202306574.

[42] Triboelectric mechanical sensors—Progress and prospects, Extreme Mech. Lett., 42, 101100. 2021, 10110010.1016/j.eml.2020.101100.

[43] Z. Wang, J. Liu, Z. Wang, C. Liu, Q. Chen, C. Zhang, W. Zhang, J. Si, X. Xiao, P. Xu, M. Xu, Highly adaptive triboelectric tactile sensor on the foot of autonomous wall-climbing robots for detecting the adhesion state and avoiding the hazard, Nano Res. (n.d.).

[44] Molecular level manipulation of charge density for solid-liquid TENG system by proton irradiation, Nano Energy 103 (2022) 107819, https://doi.org/10.1016/j.nanoen.2022.107819.

[45] Influence of temperature difference on performance of solid-liquid triboelectric nanogenerators, Nano Energy 99 (2022) 107431, https://doi.org/10.1016/j.nanoen.2022.107431.

[46] Liquid-liquid triboelectric nanogenerator based on the immiscible interface of an aqueous two-phase system | Nature Communications, (n.d.). ⟨https://www.nature.com/articles/s41467-022-33086-2⟩ (accessed September 23, 2025).

[47] Non-contact and liquid–liquid interfacing triboelectric nanogenerator for self-powered water/liquid level sensing, Nano Energy 72 (2020) 104703, https://doi.org/10.1016/j.nanoen.2020.104703.

[48] Technology Roadmap for Flexible Sensors | ACS Nano, (n.d.). ⟨https://pubs.acs.org/doi/abs/10.1021/acsnano.2c12606⟩ (accessed September 23, 2025).

[49] F. Yi, L. Lin, S. Niu, P.K. Yang, Z. Wang, J. Chen, Y. Zhou, Y. Zi, J. Wang, Q. Liao, Y. Zhang, Z.L. Wang, Stretchable-Rubber-Based triboelectric nanogenerator and its application as Self-Powered body motion sensors, Adv. Funct. Mater. 25 (2015) 3688–3696, https://doi.org/10.1002/adfm.201500428.

[50] C. Zhao, D. Liu, Y. Wang, Z. Hu, Q. Zhang, Z. Zhang, H. Wang, T. Du, Y. Zou, H. Yuan, X. Pan, J. Mi, M. Xu, Highly-stretchable rope-like triboelectric nanogenerator for self-powered monitoring in marine structures, Nano Energy 94 (2022) 106926, https://doi.org/10.1016/j.nanoen.2022.106926.

[51] C. Zhao, Q. Zhang, W. Zhang, X. Du, Y. Zhang, S. Gong, K. Ren, Q. Sun, Z.L. Wang, Hybrid piezo/triboelectric nanogenerator for highly efficient and stable rotation energy harvesting, Nano Energy 57 (2019) 440–449, https://doi.org/10.1016/j.nanoen.2018.12.062.

[52] K. Xia, Z. Xu, Applying a triboelectric nanogenerator by using facial mask for flexible touch sensor, Sens. Actuators Phys. 331 (2021) 112710, https://doi.org/10.1016/j.sna.2021.112710.

Yan Yang graduated from Baicheng Normal University in 2019 with a Bachelor of Engineering degree. Currently, he has been pursuing a master's degree under the guidance of Associate Professor Jiang Xingjia at Dalian Maritime University. His research focuses on: (1) algorithm development and application of machine learning; (2) control of sensors and robots.

Xingjia Jiang received the B.S. and M.S. degrees from Dalian Maritime University, Dalian, China, in 2007 and 2010, respectively. He has been an Associate Professor with Dalian Maritime University since 2020. His current research work focuses on energy har vesting and self-powered sensor based on triboelectric nanogenerator and intelligent ship operation and maintenance technology.

Hengxu Du is pursuing a Ph.D. in Marine Engineering at Dalian Maritime University. His research focuses on nonlinear cable vibration and structural health monitoring.

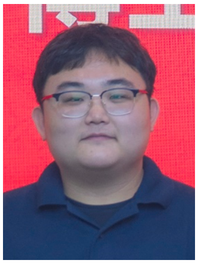

Fangyang Dong received his B.Eng. degree from Dalian Maritime University in 2019, where he is currently pursuing his Ph.D. degree under supervision of Prof. Minyi Xu since 2020. His research focuses on: (1) algorithm development and applications for machine learning and (2) hardware optimization for sensors and robots.

Mengwei Wu is a lecturer at Marine Engineering College of Dalian Maritime University. He received his Ph.D. in Engineering from Peking University. His main research interests are flow energy harvesting, flow control, and triboelectric nanogenerators. Email: wumengwei@dlmu.edu.cn

Qiang Zhao obtained his Ph.D. in Engineering from Dalian Maritime University in 2025. He was a Visiting Scholar at Peking University from 2019 to 2020. His primary research focus is on the coordination and control of underwater multi-robotic systems.

Taili Du has been with Dalian Maritime University where he is currently a professor since 2024. He received his M.S. and PhD. from Dalian Maritime University in China in 2010 and 2023. His current research work focuses on energy harvesting, self-powered sensing and AI-enabled fault diagnosis based on Triboelectric Nanogenerator.

Minyi Xu received his Ph.D. degree from Peking University in 2012. During 2016–2017, he joined Professor Zhong Lin Wang' group at Georgia Institute of Technology. Now he is a Professor in the Marine Engineering College, Dalian Maritime University. His current research is mainly focused on the areas of blue energy, self-powered systems, triboelectric nanogenerators and its practical applications in smart ship and ocean.